

Gamma-ray emission from pulsars: strength of the acceleration field in the outer gap

Kouichi Hirotani[★]

National Astronomical Observatory, Osawa, Mitaka, Tokyo 181-8588, Japan

Accepted 2000 February 19. Received 1999 November 26; in original form 1999 April 19

ABSTRACT

We study the gamma-ray emission from an outer-gap accelerator around a rotating neutron star. Assuming the existence of global currents in the magnetosphere, the charge depletion causes a large electric field along the magnetic field lines. This electric field accelerates migratory electrons and positrons, which radiate gamma-rays via curvature radiation. These gamma-rays produce radiating particles by colliding with the X-rays, maintaining a pair-production cascade in the gap accelerator. Imposing a gap-closure condition that a single pair produces one pair in the gap on average, we explicitly solve the strength of the acceleration field and demonstrate how the luminosity of the curvature-radiated, GeV photons depends on the pulsar parameters such as the surface temperature, the rotational frequency and the magnetic moment. It is predicted that J0437–4715 is a possible candidate to be detected by a next-generation gamma-ray telescope like GLAST. We further explicitly show that the TeV flux emitted from the outer gap of a typical rotation-powered pulsar is too weak to be detected by current ground-based telescopes.

Key words: magnetic fields – pulsars: individual: B0656+14 – pulsars: individual: B1055–52 – pulsars: individual: Geminga – pulsars: individual: J0437–4715 – pulsars: individual: Vela.

1 INTRODUCTION

The EGRET experiment on the *Compton Gamma Ray Observatory* has detected pulsed signals from at least six rotation-powered pulsars, which are known traditionally as radio pulsars. Interpreting γ -rays should be less ambiguous compared with non-thermal X-rays. Therefore, γ -rays are particularly important as a direct signature of basic non-thermal processes in pulsar magnetospheres and potentially should help to discriminate among different emission models.

Attempts to model the γ -ray emission have concentrated on two scenarios: polar-cap models with emission altitudes of $\sim 10^4$ cm to several neutron star radii over a pulsar polar-cap surface (Harding, Tademaru & Esposito 1978; Daugherty & Harding 1982, 1996; Dermer & Sturmer 1994; Sturmer, Dermer & Michel 1995; also see Scharlemann, Arons & Fawley 1978 for the slot-gap model) and outer-gap models with acceleration occurring in the open-field zone located near the light cylinder (Cheng, Ho & Ruderman 1986a,b, hereafter CHRa,b; Chiang & Romani 1992, 1994). Recently, Romani & Yadigaroglu (1995) developed the outer-gap models for the beaming of high-energy γ -ray emission that reproduces the observed properties of individual γ -ray pulsars. Subsequently, Romani (1996) described an emission model for

γ -ray pulsars based on curvature radiation-reaction-limited charges and estimated the efficiency of GeV photon production as a function of pulsar parameters such as pulsar age, magnetic field strength, B (G) and magnetic inclination, α_i .

However, in order to understand the γ -ray emission mechanism, the acceleration field, E_{\parallel} , in the gap is crucial. It was Hirotani & Shibata (1999a,b,c; hereafter Papers I, II and III) who first solved the spatial distribution of E_{\parallel} together with particle and γ -ray distribution functions. They explicitly demonstrated that the outer gap is formed around the null surface where the local Goldreich–Julian charge density

$$\rho_{\text{GJ}} = \frac{\Omega B_z}{2\pi c[1 - (\Omega \varpi/c)^2]} \quad (1)$$

vanishes, where B_z is the component of the magnetic field along the rotation axis, Ω refers to the angular frequency of the neutron star and ϖ indicates the distance of the point from the rotation axis. This expression for ρ_{GJ} is justified if the electric field is approximated by the corotational field or, equivalently, if the voltage drop in the gap is small compared with the available electromotive force exerted on a spinning neutron star surface, $V_* \sim 10^{15.5} \Omega^2 \mu_{30}$ V.

If the transfield thickness of the gap, D_{\perp} , is comparable with or greater than the longitudinal half width, H , then E_{\parallel} distributes quadratically having the peak at the null surface. However, if

[★]E-mail: hirotani@hotaka.mtk.nao.ac.jp

D_{\perp} is less than H , then the gap shifts outwards owing to the two-dimensional effect in the Poisson equation. For a very thin gap ($D_{\perp} \ll H$), the inner boundary approaches the null surface while the outer boundary approaches the light cylinder, of which distance from the rotation axis is given by the so-called ‘light cylinder radius’,

$$\varpi_{\text{LC}} = \frac{c}{\Omega} = 3.0 \times 10^8 \Omega_2^{-1} \text{ cm}, \quad (2)$$

where c is the speed of light and $\Omega_2 \equiv \Omega/10^2 \text{ rad s}^{-1}$. Since E_{\parallel} is shown to be kept almost constant throughout the gap in this thin case ($D_{\perp} \ll H$), this solution justifies the hypothesized gap structure in CHRa,b.

In this paper, instead of solving the spatial distribution of E_{\parallel} , we evaluate its representative value by averaging E_{\parallel} throughout the gap. Imposing a gap-closure condition that a single pair produces one pair in the gap on average, we demonstrate how the peak energy and the luminosity of γ -rays depend on parameters such as the rotation, magnetic moment and the surface temperature of the neutron star. In the next section, we consider the gap-closure condition. Solving the condition, we investigate the gap half width H and the resultant γ -ray emission from the gap in Section 3. We further apply the theory to individual pulsars in Section 4. In the final section, we discuss the validity of assumptions and consider the difference from the model of Zhang and Cheng (1997), who considered another gap-closure condition.

2 STRUCTURE OF THE GAP

2.1 Vacuum acceleration field

It is demonstrated in Paper I that there is a stationary solution for an outer gap immersed in a less dense X-ray field around a middle-aged pulsar and that the structure of the gap along the magnetic field lines is symmetric with respect to the null surface if

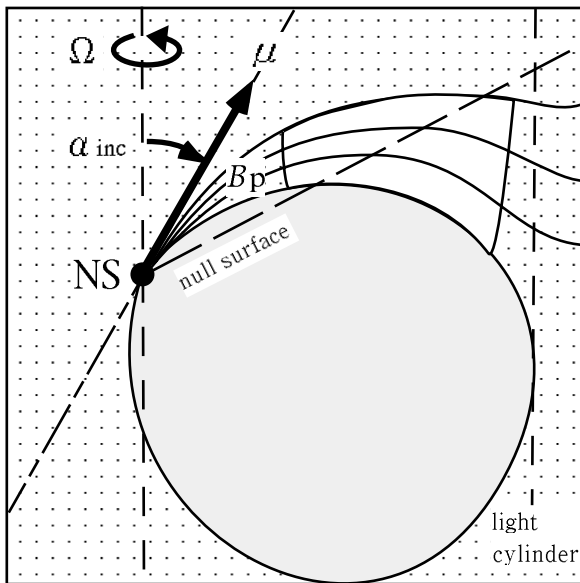


Figure 1. A side view of a hypothetical outer magnetospheric gap in which a pair-production cascade takes place. γ -ray photons are produced primarily by curvature radiation.

the transfield thickness of the gap is large in the sense of $D_{\perp} > H$. In this paper, we consider such a one-dimensional gap by introducing a rectilinear coordinate; x is an outwardly increasing coordinate along the magnetic field lines, while z is parallel to the rotational axis. We define $x = 0$ to be the intersection between the last open field line and the null surface where $B_z = 0$ (Fig. 1). Supposing the magnetic fields to be straight lines along x and approximating the null surface by the z axis, we can Taylor-expand ρ_{GJ} around $x = 0$ to obtain the following Poisson equation for the non-coriolateral potential, Φ :

$$-\frac{d^2\Phi}{dx^2} = -4\pi Ax, \quad (3)$$

where A denotes the expansion coefficient of ρ_{GJ} at the null surface ($x = 0$). Since the toroidal current flowing near the light cylinder is unknown, we simply approximate B_z with its Newtonian value. Then equation (1) gives A as follows:

$$A \equiv \frac{3\Omega\mu}{2\pi cr_0^4} \frac{1}{1 - (\Omega r_0 \sin \theta_0/c)^2} \times \left(\frac{3}{2} \sin 2\theta_0 \cos 2(\theta_0 - \alpha_i) + \cos 2\theta_0 \sin(\theta_0 - \alpha_i) \right), \quad (4)$$

where μ refers to the magnetic dipole moment of the neutron star. The position (r_0, θ_0) in the polar coordinate represents the centre of the gap ($x = 0$). They are given by

$$\frac{r_0}{\varpi_{\text{LC}}} \equiv \frac{4}{4 + \tan^2 \theta_0} \frac{2 \tan^2 \alpha_i + 3 + \sqrt{9 + 8 \tan^2 \alpha_i}}{(4/3) \tan^2 \alpha_i + 3 + \sqrt{9 + 8 \tan^2 \alpha_i}}, \quad (5)$$

$$\tan \theta_0 \equiv \frac{3 \tan \alpha_i + \sqrt{9 \tan^2 \alpha_i + 8}}{2}. \quad (6)$$

As an typical inclination, we adopt $\alpha_i = 30^\circ$ in this paper; in this case, we obtain $A = 3.19 \times 10^{-12} \Omega_2^5 \mu_{30}$, $r_0 = 0.40 \varpi_{\text{LC}}$ and $\theta_0 = 68^\circ$, where $\mu_{30} = \mu/10^{30} \text{ G cm}^3$.

Integrating equation (3), we obtain the acceleration field $E_{\parallel} \equiv -d\Phi/dx = E_{\parallel}(0) - 2\pi Ax^2$, where $E_{\parallel}(0)$ refers to the value of E_{\parallel} at $x = 0$. Defining the boundaries of the gap to be the places where E_{\parallel} vanishes, we obtain $E_{\parallel}(0) = 2\pi AH^2$. We can evaluate the typical strength of E_{\parallel} by averaging its values throughout the gap as follows:

$$\begin{aligned} \bar{E}_{\parallel} &= \frac{1}{H} \int_0^H dx (E_{\parallel}(0) - 2\pi Ax^2) \\ &= \frac{4}{3} \pi AH^2 \\ &= 3.61 \times 10^{10} \Omega_2^3 \mu_{30} \left(\frac{H}{\varpi_{\text{LC}}} \right)^2 \frac{\text{V}}{\text{m}}. \end{aligned} \quad (7)$$

In the last line, we substitute $A = 3.19 \times 10^{-12} \Omega_2^5 \mu_{30}$ esu assuming $\alpha_i = 30^\circ$.

2.2 Pair-production mean free path

The most effective assumption for the particle motion in the gap arises from the fact that the velocity saturates immediately after their birth in the balance between the radiation reaction force and the electric force. For a wide range of parameters, the reaction force is due to curvature radiation (CHRa,b; Paper I). Equating the electric force eE_{\parallel} and the radiation reaction force, we obtain the

saturated Lorentz factor at each point as follows:

$$\begin{aligned} \Gamma &= \left(\frac{3R_c^2 \bar{E}_\parallel}{2e} \right)^{1/4} \\ &= 9.59 \times 10^7 (R_{0.5}^2 \Omega_2 \mu_{30})^{1/4} \left(\frac{H}{\varpi_{\text{LC}}} \right)^{1/2}, \end{aligned} \quad (8)$$

where $R_{0.5}$ is the curvature radius R_c divided by $0.5\varpi_{\text{LC}}$ and e refers to the magnitude of the charge on the electron. In the second line, we assumed $\alpha_i = 30^\circ$. Using this Γ , we obtain the central energy of curvature radiation,

$$\begin{aligned} E_c &= \frac{3\Gamma^3 \hbar c}{2 R_c} \\ &= 174 (R_{0.5}^2 \Omega_2 \mu_{30}^3)^{1/4} \left(\frac{H}{\varpi_{\text{LC}}} \right)^{3/2} \text{ GeV}, \end{aligned} \quad (9)$$

where \hbar is the Planck constant divided by 2π . In the second line, we assumed $\alpha_i = 30^\circ$. In this paper, we adopt the grey approximation in the sense that all the γ -rays are radiated at energy E_c . In the final section, we will justify the grey approximation by comparing quantitatively with the non-grey cases (Hirotani & Shibata 1999c), in which they discarded the grey approximation and considered the γ -ray spectra explicitly to solve the Boltzmann equations for γ -rays together with those for particles and the Poisson equation for the electrostatic potential.

Let us now consider how the X-ray field determines the pair-production mean free path. First, equation (9) gives the threshold energy for soft photons to materialize as pairs by colliding with γ -rays having energy $m_e c^2 \epsilon_\gamma = E_c$,

$$E_{\text{th}} = \frac{2}{1 - \mu_c} \frac{m_e c^2}{\epsilon_\gamma}, \quad (10)$$

where μ_c refers to the cosine of the three-dimensional collisional angle between the γ -rays and the X-rays.

To evaluate μ_c , we first consider the γ -ray's toroidal momenta due to aberration. At the gap centre, the aberration angle ϕ_{abb} is given by $\tan^{-1}(r_0 \sin \theta_0 / \varpi_{\text{LC}})$. In the case of $\alpha_i = 30^\circ$, we obtain $\phi_{\text{abb}} = 20^\circ.4$. In this case, the collisional angle on the poloidal plane becomes $\theta_c = 90^\circ - \theta_0 = 21^\circ.6$ (or $\theta_c = 90^\circ + \theta_0 = 158^\circ.4$) for outwardly (respectively inwardly) propagating γ -rays. We thus obtain $\mu_c = \cos \phi_{\text{abb}} \sin \theta_c = \pm 0.345$, where the upper and the lower sign correspond to the outwardly and inwardly propagating γ -rays, respectively.

On these grounds, assuming $\alpha_i = 30^\circ$, we can rewrite equation (10) as

$$E_{\text{th}} = \frac{2.99}{1 - \mu_c} (R_{0.5}^2 \Omega_2 \mu_{30}^3)^{-1/4} \left(\frac{H}{\varpi_{\text{LC}}} \right)^{-3/2} \text{ eV}. \quad (11)$$

Let us next consider the pair-production mean free path, λ_s , for a γ -ray photon to materialize in a collision with one of the soft blackbody X-rays. If only outwardly propagating γ -rays were to contribute, λ_s would be evaluated at the gap centre ($x = 0$) as

$$\frac{1}{\lambda_{s,0}} \equiv \int_{2/(1-\mu_c)\epsilon_\gamma}^{\infty} d\epsilon_x \left(\frac{dN_s}{d\epsilon_x} \right)_0 \sigma_p(\epsilon_\gamma, \epsilon_x, \mu_c), \quad (12)$$

where $\mu_c = 0.345$ and the pair-production cross section is given

by (Berestetskii, Lifshitz & Pitaevskii 1989):

$$\begin{aligned} \sigma_p(\epsilon_\gamma, \epsilon_x, \mu_c) &\equiv \frac{3}{16} \sigma_T (1 - v^2) \left[(3 - v^4) \ln \frac{1+v}{1-v} - 2v(2 - v^2) \right], \\ v(\epsilon_\gamma, \epsilon_x, \mu_c) &\equiv \sqrt{1 - \frac{2}{1 - \mu_c} \frac{1}{\epsilon_\gamma \epsilon_x}}, \end{aligned} \quad (13)$$

σ_T is the Thomson cross section and $\epsilon_x \equiv E_x/m_e c^2$ refers to the non-dimensional energy of the X-ray photon. We may notice here that the non-dimensional threshold energy ($E_{\text{th}}/m_e c^2$) appears in the lower bound of the integral in equation (12). The number density of the soft blackbody X-rays between energies $m_e c^2 \epsilon_x$ and $m_e c^2 (\epsilon_x + d\epsilon_x)$ at the gap centre ($x = 0$) is given by the Planck law:

$$\left(\frac{dN_s}{d\epsilon_x} \right)_0 = \frac{1}{4\pi^2} \left(\frac{m_e c^2}{c\hbar} \right)^3 \left(\frac{A_s}{4\pi r_0^2} \right) \frac{\epsilon_x^2}{\exp(\epsilon_x/\Delta_s) - 1}, \quad (14)$$

where A_s indicates the observed radius of the blackbody emitting region; Δ_s is defined by

$$\Delta_s \equiv \frac{kT_s}{m_e c^2}, \quad (15)$$

where kT_s refers to the soft blackbody temperature measured by a distant observer. Since the outer gap is located outside of the deep gravitational potential well of the neutron star, the photon energy there is essentially the same as the distant observer measures.

In a realistic outer gap, not only the outwardly propagating γ -rays but also the inwardly propagating ones contribute to $\lambda_{s,0}$. Therefore, we compute $\lambda_{s,0}$ by taking an arithmetic average as follows:

$$\begin{aligned} \frac{1}{\lambda_{s,0}} &\equiv \kappa \int_{2/(1-\mu_c)\epsilon_\gamma}^{\infty} d\epsilon_x \left(\frac{dN_s}{d\epsilon_x} \right)_0 \sigma_p(\epsilon_\gamma, \epsilon_x, \mu_c) \\ &+ (1 - \kappa) \int_{2/(1+\mu_c)\epsilon_\gamma}^{\infty} d\epsilon_x \left(\frac{dN_s}{d\epsilon_x} \right)_0 \sigma_p(\epsilon_\gamma, \epsilon_x, -\mu_c). \end{aligned} \quad (16)$$

The first (respectively, the second) term represents the contribution from the outwardly (respectively, inwardly) propagating γ -rays; we adopt $\mu_c = 0.345$ for $\alpha_i = 30^\circ$.

Let us consider the weight factor, κ , which reflects the ratio of the fluxes between outwardly and inwardly propagating γ -rays. Before moving on to this task, however, it is helpful to point out that the conserved current is maintained by positrons in most portions of the gap. This can be demonstrated if we solve the Boltzmann equations for positrons and electrons by the method presented in Paper III. The solutions of the fluxes of positrons (thick curve) and electrons (thin curve) as a function of x are given in Fig. 2. The parameters are chosen to be $\alpha_i = 30^\circ$, $\Omega_2 = 0.5$, $\mu_{30} = 1.0$, $kT_s = 70$ eV and $\chi = 0.1$. The asymmetry comes from the asymmetric distribution of the X-ray density; that is, the pair-production rate decreases rapidly as the distance from the neutron star increases.

Because of the positronic dominance, the outwardly propagating γ -rays dominate the inwardly propagating ones. In Fig. 3, we present the νF_ν spectra of the outwardly (thick curve) and the inwardly (thin curve) propagating γ -rays, which are emitted by the positrons (respectively electrons) via curvature radiation; they are measured at the outer (respectively inner) boundary of the gap. The flux ratio between the outwardly and inwardly propagating γ -rays is 12 at the peak in this case. This ratio

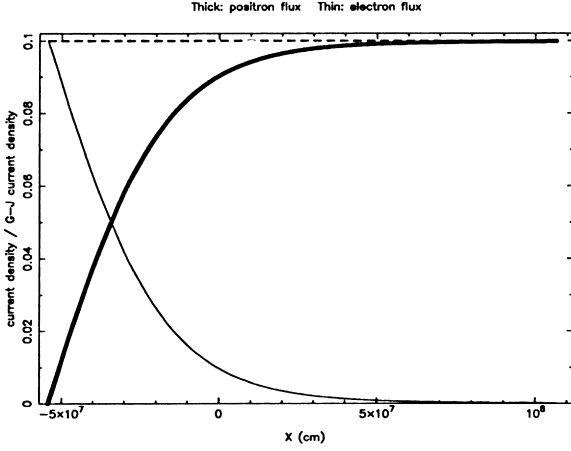


Figure 2. Positronic (thick curve) and electronic (thin curve) fluxes as a function of the position in the gap; the gap centre corresponds to the point $x = 0$. The fluxes are computed by the method presented in Paper III; parameters are chosen to be $\alpha_i = 30^\circ$, $\Omega_2 = 0.5$, $\mu_{30} = 1.0$, $kT_s = 70$ eV. The current density is set to be 10 per cent of the Goldreich–Julian value (i.e. $\chi = 0.1$ is assumed). It is assumed that no particles are injected into the gap from the boundaries.

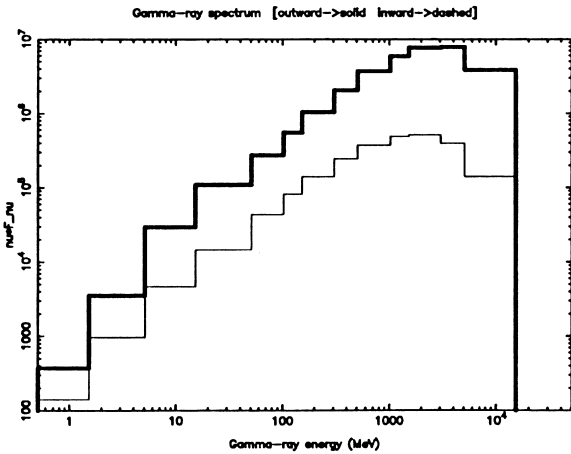


Figure 3. The νF_ν spectra of outwardly (thick curve) and inwardly (thin curve) propagating γ -rays. The ordinate is normalized arbitrarily. Synchrotron radiation, which dominates below several hundred MeV, is not included in the calculation because it is energetically negligible.

resides between 10 and 20 for a wide range of parameters $20 \text{ eV} < kT_s < 100 \text{ eV}$, $0.25 < \Omega_2 < 1.00$, $0.3 < \mu_{30} < 3.0$ and $15^\circ < \alpha_i < 45^\circ$.

In short, the flux of the outwardly propagating γ -rays is typically about ten times larger than the inwardly propagating one. Therefore, we adopt $\kappa = 0.9$ in this paper. In the final section, we justify this weight factor by comparing with the non-grey cases described in Paper III (table 3).

When the X-ray field is dominated by the blackbody radiation from the whole surface of a cooling neutron star, the true mean free path, $\lambda_{p,0}$, equals $\lambda_{s,0}$. However, it is possible that another X-ray component is emitted from limited regions of the star surface, such as heated polar caps. In this case, $\lambda_{p,0}$ can be reasonably estimated by (Beskin, Istomin & Par'ev 1992):

$$\frac{1}{\lambda_{p,0}} = \frac{1}{\lambda_{s,0}} + \frac{1}{\lambda_{h,0}}, \quad (17)$$

where $\lambda_{h,0}$ refers to the mean free path for a γ -ray photon to materialize in a collision with one of the X-rays of the additional component. If this additional component is approximately represented by a blackbody emission with temperature kT_h with an area A_h , $\lambda_{h,0}$ is given by

$$\frac{1}{\lambda_{h,0}} \equiv \kappa \int_{2/(1-\mu_c)\epsilon_\gamma}^{\infty} d\epsilon_x \left(\frac{dN_h}{d\epsilon_x} \right)_0 \sigma_p(\epsilon_\gamma, \epsilon_x, \mu_c) + (1-\kappa) \int_{2/(1+\mu_c)\epsilon_\gamma}^{\infty} d\epsilon_x \left(\frac{dN_h}{d\epsilon_x} \right)_0 \sigma_p(\epsilon_\gamma, \epsilon_x, -\mu_c). \quad (18)$$

with $\kappa = 0.9$, and the X-ray number density is evaluated at the gap centre ($x = 0$):

$$\left(\frac{dN_h}{d\epsilon_x} \right)_0 = \frac{1}{4\pi^2} \left(\frac{m_e c^2}{\hbar} \right)^3 \left(\frac{A_h}{4\pi r_0^2} \right) \frac{\epsilon_x^2}{\exp(\epsilon_x/\Delta_s) - 1}, \quad (19)$$

$$\Delta_h \equiv \frac{kT_h}{m_e c^2}. \quad (20)$$

Finally, we consider the variation of the X-ray field with the distance from the star. The X-ray densities at position x are obtained by dividing $(dN_s/d\epsilon_x)_0$ and $(dN_h/d\epsilon_x)_0$ by the factor that is proportional to the square of the distance from the star. Therefore, the local pair-production mean free path at x is given by

$$\frac{1}{\lambda_p(x, \epsilon_\gamma)} = \frac{1}{f(x/\varpi_{LC})} \int_{2/(1-\mu_c)\epsilon_\gamma}^{\infty} d\epsilon_x \left[\left(\frac{dN_s}{d\epsilon_x} \right)_0 + \left(\frac{dN_h}{d\epsilon_x} \right)_0 \right] \sigma_p, \quad (21)$$

where

$$f(a) \equiv 1 + 2a \sin \theta_0 + a^2 \quad (22)$$

represents the variation of the X-ray density with $x (= a \varpi_{LC})$.

2.3 Gap closure

The gap width $2H$ is adjusted so that a single pair produces copious γ -ray photons (of number N_γ), one of which materializes as a pair on average. Since a typical γ -ray photon runs the length H in the gap before escaping from either of the boundaries, the probability of a γ -ray photon to materialize within the gap, N_γ^{-1} , must coincide with the optical depth for absorption, H/λ_p . Considering the position dependence of λ_p on x , we obtain the following gap-closure condition:

$$\frac{1}{N_\gamma} = \frac{1}{2} \int_{-H}^H \frac{dx}{\lambda_p}, \quad (23)$$

where

$$N_\gamma \approx \frac{H}{c} \frac{4e^2 \Gamma}{9\hbar R_c} = 6.22 \times 10^5 \left(\frac{\Omega_2 \mu_{30}}{R_{0.5}^2} \right)^{1/4} \left(\frac{H}{\varpi_{LC}} \right)^{3/2}. \quad (24)$$

It follows that the optical depth for pair production, N_γ^{-1} , is much less than unity (see Section 5 for details).

Substituting equation (21) into (23), we obtain

$$\frac{1}{N_\gamma} = \frac{H}{\lambda_{p,0}} I \left(\frac{H}{\varpi_{LC}} \right), \quad (25)$$

where $\lambda_{p,0}$ is defined by equation (17) and

$$I(h) \equiv \frac{\tan^{-1}(\tan \theta_0 + h \sec \theta_0) - \tan^{-1}(\tan \theta_0 - h \sec \theta_0)}{2h \cos \theta_0}. \quad (26)$$

For a very thin gap ($h = H/\varpi_{\text{LC}} \ll 1$), $I(h)$ approaches unity. Combining equations (17), (25) and (24), we finally obtain the equation that describes H/ϖ_{LC} as a function of B_5 , Ω_2 , kT_s , A_s , kT_h and A_h .

2.4 Gamma-ray luminosity

Let us first consider the luminosities of curvature-radiated γ -rays. Remembering the fact that most of the γ -rays are emitted by positrons, we can estimate the luminosity of the curvature-radiated γ -rays, L_{GeV} , by multiplying the total number of positrons in the gap, N_e , the number of γ -rays emitted per unit time by a single positron (or almost equivalently by a single pair), $N_\gamma/(H/c)$, and the γ -ray energy, E_c . That is, we have

$$L_{\text{GeV}} = N_e \times \frac{N_\gamma}{H/c} \times E_c. \quad (27)$$

Evaluating the conserved current density by $\chi(\Omega B/2\pi e)$, where $(\Omega B/2\pi e)$ refers to the Goldreich–Julian number density, and assuming that the gap extends $\pi(H/\varpi_{\text{LC}})$ rad in the azimuthal direction, we obtain

$$N_e \sim \chi \frac{\Omega B}{2\pi c e} \cdot \frac{\pi H}{\varpi_{\text{LC}}} \cdot r_0 \sin \theta_0 \cdot D_\perp \cdot 2H. \quad (28)$$

The distance of the centre of the gap from the rotation axis, $r_0 \sin \theta_0$, becomes $0.37\varpi_{\text{LC}}$ for $\alpha_i = 30^\circ$. Substituting equations (9), (24) and (28) into (27), we obtain

$$L_{\text{GeV}} \sim 1.19 \times 10^{39} \left(\chi \frac{D_\perp}{\varpi_{\text{LC}}} \right) \Omega_2^4 \mu_{30}^2 \left(\frac{H}{\varpi_{\text{LC}}} \right)^4 \text{ ergs s}^{-1}. \quad (29)$$

In Papers I, II and III it is demonstrated that stationary solutions exist even when D_\perp becomes comparable with H . We thus assume a transversely thick outer gap with $D_\perp = 0.3\varpi_{\text{LC}}$. If D_\perp is much less than this value, as assumed in CHRa,b, the γ -ray luminosity becomes much less than would be obtained under $D_\perp = 0.3\varpi_{\text{LC}}$. As for χ , its maximum values will be about 0.2 for a wide range of values of the parameters kT_s , Ω and μ (Papers I, II, III), provided that no particles enter from the boundaries. If particles enter from the boundaries, χ is allowed to be as large as unity. However, $\chi \sim 1$ violates the assumption of the vacuum gap; therefore, we assume $\chi \sim 0.1$ in this paper.

Secondly, let us consider the luminosity of Compton-scattered γ -rays, L_{TeV} . We should notice here that it is the infrared photons with energy ~ 0.1 eV that contribute most effectively as the target photons of inverse Compton (IC) scattering. Neither the higher energy photons, such as surface blackbody X-rays, nor the lower energy photons, such as those from polar radio emission, contribute as the target photons, because either they have cross sections that are too small or the energy transfer when they are scattered is too small. The collisional frequency for a particle to scatter inversely the infrared photons of number density $N_{0.1\text{eV}}$ is given by $cN_{0.1\text{eV}}\sigma_T$. Considering the fact that the maximum energy of the scattered photons is $\Gamma m_e c^2$, we can evaluate the upper limit of the TeV emission as

$$\begin{aligned} L_{\text{TeV}} &< N_e \times cN_{0.1\text{eV}}\sigma_T \times \Gamma m_e c^2 \\ &= 1.25 \times 10^{35} \left(\chi \frac{D_\perp}{\varpi_{\text{LC}}} \right) \Omega_2^{13/4} \mu_{30}^{5/4} R_{0.5}^{1/2} L_{30} \\ &\times \left(\frac{H}{\varpi_{\text{LC}}} \right)^{5/2} \text{ ergs s}^{-1}, \end{aligned} \quad (30)$$

where L_{30} refers to the luminosity of infrared photons that can be scattered up to TeV energy range in units of 10^{30} ergs s^{-1} . The ratio between L_{TeV} and L_{GeV} then becomes

$$\frac{L_{\text{TeV}}}{L_{\text{GeV}}} < 1.04 \times 10^{-4} L_{30} \left(\frac{R_{0.5}^2}{\Omega_2^3 \mu_{30}^3} \right)^{1/4} \left(\frac{H}{\varpi_{\text{LC}}} \right)^{-3/2}. \quad (31)$$

It follows that TeV luminosities are much less than GeV ones for moderate values of parameters. The effect of pair production due to TeV–eV photon collisions is, therefore, self-consistently negligible compared with that due to GeV–keV collisions.

3 GAMMA-RAY RADIATION VERSUS SURFACE BLACKBODY TEMPERATURE

Once H/ϖ_{LC} is obtained from equation (25), we can compute all other quantities by using equations (7)–(10) and (24)–(30). To this aim, we first show the results of H/ϖ_{LC} as a function of kT_s , Ω and μ in Section 3.1. We then study the voltage drop in the gap in Section 3.2 and the γ -rays emission in Section 3.3. Throughout this section, we assume that the X-rays illuminating the gap are emitted from the whole neutron star surface. Therefore, we neglect the presence of the hard blackbody component and put $\lambda_h = \infty$ in equation (17) and $A_s = A_* \equiv 4\pi r_*^2$ in equation (14) in this section, where r_* refers to the neutron star radius and is supposed to be 10 km in this paper. Such a situation will be realized if most of the hard X-rays emitted from heated polar caps are scattered back to the stellar surface owing to cyclotron resonance scatterings and re-emitted as soft X-rays (Daugherty & Harding 1989; Halpern & Ruderman 1993).

3.1 Gap half width

Solving equation (25) for H/ϖ_{LC} , we obtain the gap half width as a function of kT_s . The results are presented in Fig. 4. The thick solid, dashed, dotted lines correspond to $\mu_{30} = 1.0, 3.0$ and 0.3 with $\Omega_2 = 0.5$, respectively, while the thin dashed and dotted ones to $\Omega_2 = 0.75$ and 0.25 with $\mu = 1.0$. The curvature radius is fixed as $R_{0.5} = 1.0$.

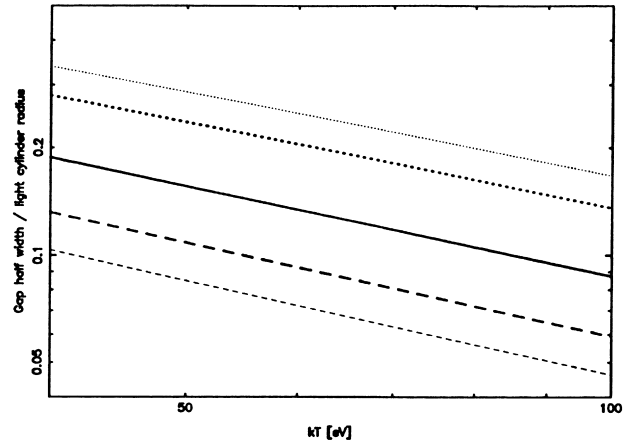


Figure 4. Examples of the gap half width, H , divided by the light cylinder radius, ϖ_{LC} , as a function of kT_s , Ω and B . Both the abscissa and the ordinate are in logarithmic scales. The thick solid, dashed and dotted lines correspond to $(\Omega_2, \mu_{30}) = (0.5, 1.0)$, $(0.5, 3.0)$ and $(0.5, 0.3)$, respectively, while the thin dashed and dotted lines correspond to $(1.0, 1.0)$ and $(0.25, 1.0)$, respectively.

First of all, it follows from the figure that H/ϖ_{LC} is a decreasing function of kT_s . The reason is as follows: if kT_s increases, the number density of target soft photons $N_s(E > E_{\text{th}})$ above threshold for pair production increases for a fixed value of E_{th} . The increased $N_s(E > E_{\text{th}})$ results in the decrease of λ_p , which reduces H (equation 25). For more accurate discussion, we must take account of the fact that the resultant increase of E_{th} partially cancels the reduction of H : the reduced H results in a decrease of E_{\parallel} and hence E_c . This in turn increases E_{th} to decrease $N_s(E > E_{\text{th}})$; as a result, λ_p partially increases. In addition, the reduction of H implies the reduction in the emitting length for a particle, thereby decreasing N_γ to partially cancel the initial decrease of H through equation (25). Nevertheless, both of the two effects are passive; therefore, the nature of the decrease of H with increasing kT_s is unchanged.

The three thick lines in Fig. 4 indicate that H/ϖ_{LC} decreases with increasing μ . This is because the expansion coefficient A (equation 3) increases with increasing μ . That is, the increase of A results in a strong acceleration field (see next subsection) with a small gap width.

The three thin lines indicate that H/ϖ_{LC} decreases with increasing Ω . For a large Ω , the gap shrinks to increase the photon density $N_s(E > E_{\text{th}})$, which decreases H .

From the numerical results, a useful approximated solution can be obtained as follows:

$$\frac{H}{\varpi_{\text{LC}}} = 0.0484\Omega_2^{-0.85}\mu_{30}^{-0.36}\left(\frac{kT_s}{100\text{eV}}\right)^{-0.83}. \quad (32)$$

The error is within 6 per cent in the parameter range $0.25 < \Omega_2 < 1.0$, $0.3 < \mu_{30} < 3.0$ and $20\text{eV} < kT_s < 100\text{eV}$. The lower bound of kT_s is determined so that $H < 0.5\varpi_{\text{LC}}$ may hold, whereas the upper bound comes from the requirement that the particles be mono-energetic.

3.2 Acceleration field and voltage drop

The representative value of the acceleration field, E_{\parallel} , can be readily computed from equations (7) and (32). The result is

$$\bar{E}_{\parallel} = 8.7 \times 10^7 \Omega_2^{1.29} \mu_{30}^{0.28} \left(\frac{kT_s}{100\text{eV}}\right)^{-1.67} \frac{\text{V}}{\text{m}}. \quad (33)$$

Thus, the terminal Lorentz factor becomes as large as

$$\Gamma = 2.1 \times 10^7 \Omega_2^{-0.18} \mu_{30}^{0.07} R_{0.5}^{0.5} \left(\frac{kT_s}{100\text{eV}}\right)^{-0.42}. \quad (34)$$

The dependences on μ are very small. Note that both E_{\parallel} and Γ decrease with increasing kT_s .

The voltage drop in the gap, $V_{\text{gap}} = \bar{E}_{\parallel} \cdot H$, is given by

$$V_{\text{gap}} \equiv \frac{8}{3} \pi A H^3 = 1.9 \times 10^{17} \Omega_2^2 \mu_{30} \left(\frac{H}{\varpi_{\text{LC}}}\right)^3 \text{V}. \quad (35)$$

It follows that for a cooling neutron star having a temperature as small as $\sim 40\text{eV}$, $H \sim 0.2\varpi_{\text{LC}}$ gives $V_{\text{gap}} \sim 10^{15}\text{V}$; this corresponds to roughly 30 per cent of V_* , the surface EMF. To sum up, more spin-down luminosity will be converted into γ -ray emission for older pulsars, because

$$\frac{V_{\text{gap}}}{V_*} = 6.8 \times 10^{-3} \Omega_2^{-2.6} \mu_{30}^{-1.1} \left(\frac{kT_s}{100\text{eV}}\right)^{-2.5} \quad (36)$$

increases with decreasing Ω_2 and kT_s .

3.3 Curvature radiation

Let us next consider the energy and luminosity of curvature radiation. Substituting equation (32) into (9), we obtain

$$E_c = 1.9 \Omega_2^{0.47} \mu_{30}^{0.21} R_{0.5}^{0.5} \left(\frac{kT_s}{100\text{eV}}\right)^{-1.3} \text{GeV}. \quad (37)$$

When kT_s is as high as 100 eV, E_c becomes typically a few GeV. However, if the neutron star cools down to $kT_s \sim 20\text{eV}$, it becomes as large as 12 eV. For a realistic neutron star, not only kT_s but also Ω_2 become small as it evolves; thus, the tendency of growing E_c with age will be partially cancelled due to the decrease of Ω .

Substituting the results of H/ϖ_{LC} into equation (29), we obtain the γ -ray luminosity due to curvature radiation as

$$L_{\text{GeV}} = 2.0 \times 10^{32} \left(\frac{\chi}{0.1} \frac{D_{\perp}}{0.3\varpi_{\text{LC}}}\right) \Omega_2^{0.59} \mu_{30}^{0.56} \times \left(\frac{kT_s}{100\text{eV}}\right)^{-3.33} \text{ergs s}^{-1}. \quad (38)$$

We can conclude that both the peak energy and the luminosity of the GeV γ -rays are a decreasing function of kT_s . This fact is deeply related to the increase of target X-ray photons for pair production with increasing kT_s .

3.4 Inverse Compton scattering

The relativistic particles produce γ -rays mainly via curvature radiation as described in the preceding sections. However, even though energetically negligible, it is useful to draw attention to the TeV γ -rays produced via IC scatterings. First, it follows from equations (32) and (8) that the upper cut-off energy of TeV γ -rays is given by

$$\Gamma m_e c^2 = 10.8 \Omega_2^{-0.18} \mu_{30}^{0.07} R_{0.5}^{0.5} \left(\frac{kT_s}{100\text{eV}}\right)^{-0.42} \text{TeV}. \quad (39)$$

Therefore, the upper cut-off energy virtually depends on the surface temperature, kT_s .

Secondly, substituting the relation (32) into (30), we obtain the γ -ray luminosity due to IC scatterings as

$$L_{\text{TeV}} < 1.9 \times 10^{30} \left(\frac{\chi}{0.1} \frac{D_{\perp}}{0.3\varpi_{\text{LC}}}\right) \Omega_2^{1.11} \mu_{30}^{0.35} R_{0.5}^{0.5} L_{30} \times \left(\frac{kT_s}{100\text{eV}}\right)^{-2.08} \text{ergs s}^{-1}. \quad (40)$$

We can see that both the cut-off energy and the luminosity of TeV γ -rays are a decreasing function of kT_s for the same reason as GeV emission.

4 APPLICATION TO INDIVIDUAL PULSARS

In this section, we apply the theory to six pulsars. We present in Table 1 their observed X-ray properties in order of spin-down luminosity, \dot{E}_{rot} .

(i) **Vela**. From *ROSAT* observations in the 0.06–2.4 keV band, the spectrum of its point source (presumably the pulsar) emission is expressed by two components: a surface blackbody component with $kT_s = 150\text{eV}$ and $A_s = 0.066A_* d_{0.5}^2$ and a power-law

Table 1. Input X-ray field.

Pulsar	$\log_{10} \dot{E}_{\text{rot}}$ $\text{lg}(\text{erg s}^{-1})$	Distance kpc	Ω rad s^{-1}	$\log_{10} \mu$ $\text{lg}(\text{G cm}^3)$	kT_s keV	A_s/A_*	kT_h keV	A_h/A_*
Vela	36.84	0.50	61.3	30.53	150	0.066	–	–
B0656+14	34.58	0.76	15.3	30.67	67	4.5	129	$10^{-1.49}$
Geminga	34.51	0.16	26.5	30.21	48	0.16	–	–
B1055–52	34.48	1.53	31.9	30.03	68	7.3	320	$10^{-3.64}$
J0437–4715	33.60	0.178	1092	26.50	28	0.014	106	$10^{-2.28}$

Table 2. Expected properties of curvature-radiated γ -rays.

Pulsar	$P_{\text{curv}}/P_{\text{IC}}$	l_{acc}/H	H/ϖ_{LC}	E_c GeV	L_{GeV}^a erg s^{-1}	L_{GeV}^a/d^2 $\text{erg s}^{-1} \text{cm}^{-2}$	$\Gamma m_e c^2$ TeV	$L_{\text{TeV}}/L_{\text{GeV}}$
Vela	7.4×10^6	0.70	0.052	2.0	3.7×10^{32}	1.6×10^{-10}	13.2	$< 3.3 \times 10^{-3} L_{30}^b$
B0656+14	5.8×10^6	0.33	0.16	1.4	3.2×10^{32}	5.9×10^{-11}	18.3	$< 2.0 \times 10^{-3} L_{30}$
Geminga	5.6×10^8	0.073	0.28	3.7	3.0×10^{33}	1.3×10^{-8}	21.1	$< 1.2 \times 10^{-3} L_{30}$
B1055–52	1.1×10^6	0.45	0.13	1.2	1.4×10^{32}	6.7×10^{-12}	13.8	$< 4.6 \times 10^{-3} L_{30}$
J0437–4715	1.5×10^8	0.053	0.31	4.6	4.6×10^{32}	1.5×10^{-9}	6.6	$< 4.2 \times 10^{-2} L_{30}$

^a The GeV emissions are assumed to be beamed in 1 steradian.

^b L_{30} indicates the infrared luminosity in the unit of $10^{30} \text{ erg s}^{-1}$.

component with a photon index of -3.3 . However, the latter component does not show pulsations; therefore, we consider only the former component as the X-ray field illuminating the outer gap.

(ii) **B0656+14.** Combining *ROSAT* and *ASCA* data, Greiveldinger et al. (1996) reported that the X-ray spectrum consists of three components: the soft surface blackbody component with $kT_s = 67 \text{ eV}$ and $A_s = 4.5A_*d_{0.76}^2$ at a distance of 760 pc, a hard blackbody component due to polar-cap heating with $kT_h = 129 \text{ eV}$ and $A_h = 3.2 \times 10^{-2}A_*d_{0.76}^2$, and a power-law component with a photon index of -1.5 . Since the area of the heated polar cap is relatively large, the hard blackbody component takes the major role in maintaining the gap; we thus neglect the power-law component and use equation (17) to compute λ_p .

(iii) **Geminga.** The X-ray spectrum consists of two components: the soft surface blackbody component with $kT_s = 48 \text{ eV}$ and $A_s = 0.16A_*d_{0.16}^2$, and a hard power-law component with a photon index of -1.6 (Halpern & Wang 1997). However, the latter component is negligible, because H/ϖ_{LC} is overestimated by only 0.3 per cent if we compute λ_p from the former component alone. A parallax distance of 160 pc was estimated from *HST* observations (Caraveo et al. 1996).

(iv) **B1055–52.** Combining *ROSAT* and *ASCA* data, Greiveldinger et al. (1996) reported that the X-ray spectrum consists of two components: the soft blackbody component with $kT_s = 68 \text{ eV}$ and $A_s = 7.3A_*d_{1.53}^2$ and a hard blackbody component due to polar-cap heating with $kT_h = 320 \text{ eV}$ and $A_h = 2.3 \times 10^{-4}A_*d_{1.53}^2$.

(v) **J0437–4715.** Using *ROSAT* and *EUVE* data (Becker & Trümper 1993; Halpern and Ruderman 1996), Zavlin and Pavlov (1998) demonstrated that both the spectra and the light curves of its soft X-ray radiation can originate from hot polar caps with a non-uniform temperature distribution and be modelled by step-like functions having two different temperatures. The first component is the emission from a heated polar-cap core with temperature $kT_h = 140_{-45}^{+15} \text{ eV}$ measured at the surface and with an area $A_h = (7.2_{-1.6}^{+32.8}) \times 10^{-4}A_*$. The second component can be interpreted as a cooler rim around the polar cap on the neutron star surface with temperature $kT_s = 37_{-11}^{+6} \text{ eV}$ and with an area $A_s = (1.4_{-0.4}^{+7.6}) \times 10^{-2}A_*$. Considering a gravitational redshift factor of 0.76, the best-fit temperatures observed at infinity become $kT_s = 28 \text{ eV}$ and $kT_h = 106 \text{ eV}$. From parallax measurements, its

distance is reported to be $178 \pm 26 \text{ pc}$ (Sandhu et al. 1997). We adopt $d = 180 \text{ pc}$ as a representative value.

For all the five pulsars, the radiative reaction force is dominated by the curvature process rather than the IC scatterings, because $P_{\text{curv}}/P_{\text{IC}}$ is much greater than unity. Moreover, the acceleration length, l_{acc} is less than the gap half width, H ; therefore, the particle distribution can be considered to be mono-energetic in the first order of approximation. As for the central energy of curvature radiation, E_c , it follows that the GeV spectrum of J0437–4715 and Geminga should be much harder than Vela, B0656+14 and B1055–52. The reason that Geminga has hard GeV spectra is that its number density of X-rays at the gap is significantly smaller compared with the latter three pulsars. For the millisecond pulsar J0437–4715, its very small curvature radius R_c results in the hard curvature radiation.

Moreover, we obtain the expected GeV fluxes of individual pulsars by dividing L_{GeV} by d^2 . It follows from the seventh column that J0437–4715 is a possible candidate to be observed in a future mission. The properties of E_c and L_{GeV} will be able to be checked by GLAST, which will help us to discriminate among different models of high-energy emission from pulsar magnetospheres.

Let us finally point out the fact that L_{TeV} is much less than L_{GeV} (the last column in Table 2). It follows that the TeV emissions from the outer gaps of these five rotation-powered pulsars are unobservable with the current ground-based telescopes. It is noteworthy that the same conclusion can be derived if we discard the gap closure condition (equation 23) and solve instead the Vlasov equations describing the gap under appropriate boundary conditions (Hirotani 2000).

5 SUMMARY AND DISCUSSION

In summary, for pulsars whose X-ray field at the outer-gap is dominated by surface blackbody radiation, the curvature process dominates inverse Compton scattering to limit the particle Lorentz factor below 5×10^7 . Imposing the gap-closure condition that a single pair produces one pair in the gap on average, we can solve the gap width as a function of kT_s , Ω and μ ; this allows us to compute further other quantities such as the energy and the

luminosity of γ -ray radiation. It is demonstrated that the central energy (E_c) and the luminosity (L_{GeV}) of curvature radiation and the cut-off energy ($\Gamma m_e c^2$) and the luminosity (L_{TeV}) of inverse Compton scattering increase with decreasing surface temperature (kT_s); this is because the X-ray density decreases with decreasing kT_s . It should be noted that TeV fluxes for typical pulsar parameters are negligibly small compared with the GeV fluxes and hence difficult to detect using current ground-based telescopes.

To discuss the relationship between L_γ and the spin-down luminosity, we must know how the current flowing in the gap depends on μ and Ω . However, the current, which is proportional to $ceN_e D_\perp \propto \chi D_\perp$, should be decided by a global condition in the magnetosphere rather than by a local condition in the gap (Shibata 1995). Thus, we will not discuss this topic further.

Let us show the validity of assumptions that have been made in this paper. First, we check whether the gap width does not exceed the light cylinder radius. It follows from Fig. 4 that H/ϖ_{LC} exceeds 0.5 at $kT_s = 20$ eV for a small Ω ($\approx 25 \text{ rad s}^{-1}$) or a small μ ($\approx 3 \times 10^{29} \text{ G cm}^3$). We thus set the lower bound of kT_s to be 20 eV in Fig. 4.

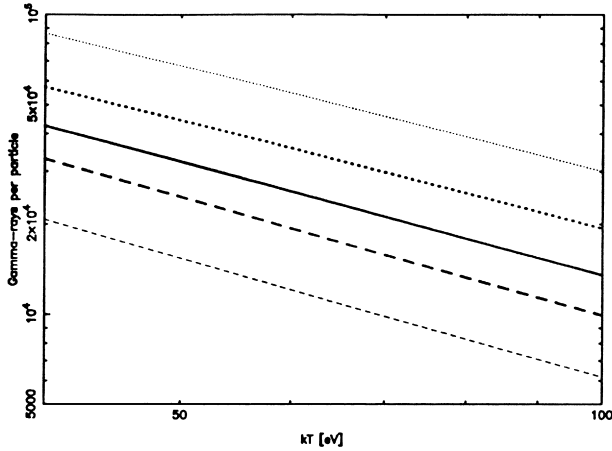


Figure 5. The average number of γ -rays radiated by a single particle during its migration in the whole gap. Both the abscissa and the ordinate are in logarithmic scales. The five curves correspond to the same parameter sets as in Fig. 2.

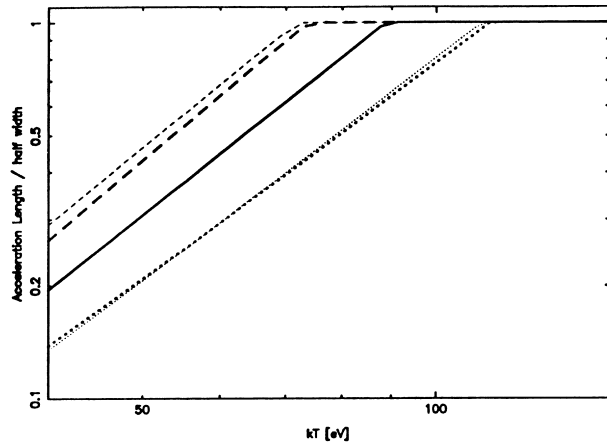


Figure 6. Acceleration length divided by the gap half width as a function of the surface temperature. Both the abscissa and the ordinate are in logarithmic scales. The parameters are chosen to be typical for millisecond pulsars (see text).

Secondly, we must check that the acceleration length, l_{acc} , is sufficiently less than H so that most of the particles attain the terminal Lorentz factor (equation 8). Substituting equations (7) and (8) into $l_{\text{acc}} = \Gamma m_e c^2 / eE_\parallel$, we obtain

$$\frac{l_{\text{acc}}}{H} = 5.1 \times 10^{-4} (R_{0.5}^2 \Omega_2^{-7} \mu_{30}^{-3})^{1/4} \left(\frac{H}{\varpi_{\text{LC}}} \right)^{-5/2}. \quad (41)$$

Substituting the results of H/ϖ_{LC} (Fig. 4) into this equation, we find that $l_{\text{acc}} < H$ is satisfied for $kT_s < 100$ eV. Therefore, we adopt the upper limit of kT_s as 100 eV in the figure.

Thirdly, it is worth noting that the optical depth for pair production within the gap, $H/\lambda_p = N_\gamma^{-1}$, is kept well below unity. This condition is necessary for the gap closure relation (25) to be justified. Substituting the results of H/ϖ_{LC} (Fig. 4) into equation (24), we obtain N_γ as a function of Ω , μ and kT_s as depicted in Fig. 5. It follows from Fig. 5 that N_γ^{-1} is always much less than unity for $\Omega > 25 \text{ rad s}^{-1}$, $\mu < 3 \times 10^{30} \text{ G cm}^3$ and $20 \text{ eV} < kT_s < 100 \text{ eV}$. In other words, the condition $l_{\text{acc}} \ll H$ is much more severe than $N_\gamma^{-1} \ll 1$.

The same can be said for the parameter set of a typical millisecond pulsar. In Fig. 6, we present the results of l_{acc}/H as a function of kT_s . For the three thick curves, Ω is fixed at 10^3 rad s^{-1} ; the solid, dashed and dotted curves are assigned $\mu = 10^{27}$, 10^{28} and 10^{26} G cm^3 , respectively. The thin dashed and dotted curves correspond to $\Omega = 2 \times 10^3$ and $5 \times 10^2 \text{ rad s}^{-1}$, respectively; μ is fixed at 10^{27} G cm^3 . It follows from Fig. 6 that the applicable range of kT_s is bounded as

$$kT_s < 90 \text{ eV} \left(\frac{\mu}{10^{27} \text{ G cm}^3} \right)^{-0.1} \left(\frac{\Omega}{10^3 \text{ rad s}^{-1}} \right)^{-0.33} \quad (42)$$

by the requirement of $l_{\text{acc}} < H$. On the other hand, the optical depth

$$N_\gamma^{-1} \sim 10^{-3.5} \left(\frac{kT_s}{100 \text{ eV}} \right)^{1.2} \left(\frac{\mu}{10^{27} \text{ G cm}^3} \right)^{0.3} \times \left(\frac{\Omega}{10^3 \text{ rad s}^{-1}} \right)^{1.2} \quad (43)$$

is kept much less than unity also for millisecond pulsars as long as kT_s is below the upper bound (equation 42).

Fourthly, we can check the validity of the grey approximation adopted in the present paper by comparing the results with those obtained in the non-grey analysis in which the energy spectra of γ -rays are explicitly considered. Such a non-grey analysis was

Table 3. This work versus non-grey cases.

α_i	Ω rad s $^{-1}$	μ G cm 3	kT_s eV	H/ϖ_{LC}	
				This work	Non-grey a
30°	50	10^{30}	70	0.117	0.116
30°	50	3×10^{30}	70	0.080	0.086
30°	50	3×10^{29}	70	0.180	0.161
30°	25	10^{30}	70	0.221	0.202
30°	100	10^{30}	70	0.063	0.067
30°	300	10^{28}	70	0.117	0.101
30°	1000	10^{27}	70	0.088	0.072
30°	50	10^{30}	40	0.187	0.187
30°	50	10^{30}	100	0.087	0.085
0°	50	10^{30}	70	0.241	0.191
15°	50	10^{30}	70	0.180	0.156
45°	50	10^{30}	70	0.062	0.066
60°	50	10^{30}	70	0.022	0.058

a The non-grey cases are calculated by the method presented in Paper III.

performed in Paper III, in which the distribution functions of the γ -rays and particles and the acceleration field $E_{\parallel}(x) \equiv -d\Phi(x)/dx$ were examined by solving simultaneously the Boltzmann equations for γ -rays and particles and the Poisson equation for the potential $\Phi(x)$. The results of H/ϖ_{LC} computed from the present grey analysis and the non-grey one in Paper III are compared in Table 3. It follows from the table that the grey approximation gives good estimates of H/ϖ_{LC} as the first order approximation, provided that $15^\circ < \alpha_i < 45^\circ$ holds. For a highly oblique rotator ($\alpha_i \sim 60^\circ$), the grey approximation (equation 9) adopted in this paper gives too small a gap width.

ACKNOWLEDGMENTS

This research owes much to the helpful comments of Dr S. Shibata. The author wishes to express his gratitude to Drs A. Harding and Y. Saito for valuable advice. He also thanks the Astronomical Data Analysis Center of the National Astronomical Observatory, Japan, for the use of workstations.

REFERENCES

- Becker W., Trümper J., 1993, *Nat*, 365, 528
 Becker W., Trümper J., 1996, *A&AS*, 120, 69
 Becker W., Trümper J., 1997, *A&A*, 326, 682
 Berestetskii V. B., Lifshitz E. M., Pitaevskii L. P., 1989, *Quantum Electrodynamics*, Landau Lifshitz Course of Theoretical Physics, Vol. 4, 2nd edn. Pergamon Press, Oxford, Section 89
 Beskin V. S., Istomin Ya.N., Par'ev V. I., 1992, *Sov. Astron.*, 36, 6, 642
 Caraveo P. A., Bignami G. F., Mignani R., Taff L. G., 1996, *ApJ*, 461, L91
 Cheng K. S., Ho C., Ruderman M., 1986a, *ApJ*, 300, 500 (CHRa)
 Cheng K. S., Ho C., Ruderman M., 1986b, *ApJ*, 300, 522 (CHRb)
 Chiang J., Romani R. W., 1992, *ApJ*, 400, 629
 Chiang J., Romani R. W., 1994, *ApJ*, 436, 754
 Daugherty J. K., Harding A. K., 1982, *ApJ*, 252, 337
 Daugherty J. K., Harding A. K., 1989, *ApJ*, 336, 861
 Daugherty J. K., Harding A. K., 1996, *ApJ*, 458, 278
 Dermer C. D., Sturmer S. J., 1994, *ApJ*, 420, L75
 Fierro J. M., Michelson P. F., Nolan P. L., Thompson D. J., 1998, *ApJ*, 494, 734
 Greiveldinger C. et al., 1996, *ApJ*, 465, L35
 Halpern J. P., Ruderman M. A., 1993, *ApJ*, 415, 286
 Harding A. K., Tadamaru E., Esposito L. S., 1978, *ApJ*, 225, 226
 Hirovani K., 2000, *PASJ*, 52, 1
 Hirovani K., Shibata S., 1999a, *MNRAS*, 308, 54 (Paper I)
 Hirovani K., Shibata S., 1999b, *MNRAS*, 308, 67 (Paper II)
 Hirovani K., Shibata S., 1999c, *PASJ*, 51, 5, 683 (Paper III)
 Romani R. W., 1996, *ApJ*, 470, 469
 Romani R. W., Yadigaroglu I. A., 1995, *ApJ*, 438, 314
 Sandhu J. S. et al., 1997, *ApJ*, 478, L95
 Scharlemann E. T., Arons J., Fawley W. T., 1978, *ApJ*, 222, 297
 Shibata S., 1995, *MNRAS*, 276, 537
 Sturmer S. J., Dermer C. D., Michel F. C., 1995, *ApJ*, 445, 736
 Zavlin V. E., Pavlov G. G., 1998, *A&A*, 329, 583
 Zhang L., Cheng K. S., 1997, *ApJ*, 487, 370

This paper has been typeset from a $\text{\TeX}/\text{\LaTeX}$ file prepared by the author.